GEOFIZIKA VOL. 30 2013

Professional paper
UDC 550.34.013

A fourth-order accurate finite-difference program for the simulation of SH-wave propagation in heterogeneous viscoelastic medium

J. P. Narayan and Vinay Kumar

Indian Institute of Technology Roorkee, Department of Earthquake Engineering, Roorkee, India

Received 11 August 2013, in final form 14 September 2013

This article presents a staggered grid time-domain finite-difference (FD) program for the simulation of SH-wave propagation in a viscoelastic heterogeneous medium. The incorporation of realistic damping in FD program is based on a rheological model widely known as generalized Maxwell body (GMB-EK). The accuracy of implementation of realistic damping is validated by comparing the numerically computed frequency dependent quality factors and phase velocity with the same computed using GMB-EK rheological model and the Futterman's relationship. The accuracy was also validated by comparing the numerically computed soil amplification at resonance frequency for different damping with the analytical solutions. The stability and grid dispersion are also studied in details.

Keywords: viscoelastic SH-wave equations, finite difference program, fourth order spatial accuracy, VGR-stress imaging technique, and stability and grid dispersion

1. Introduction

Realistic quantification of local site effects on the ground motion characteristics requires an efficient numerical method (Narayan, 2003; Narayan and Rao, 2003; Narayan, 2005; 2010; 2012). The staggered-grid fourth-order accurate finite-difference (FD) method, proposed by Madariaga (1976), is one of the most useful numerical methods to simulate the ground motion characteristics (Levander, 1988; Graves, 1996; Moczo et al., 2002; Narayan and Kumar, 2008). The accuracy of time domain FD method very much depends on the implementation of realistic damping in the simulations. The behavior of real earth material is viscoelastic in nature and is responsible for frequency dependent damping of seismic waves. Seismic data suggest that the internal friction of rock (a measure of attenuation 'Q^{-1}') is nearly independent of frequency, at least over more than three decades of frequency (McDonal et. al., 1958; Liu et al., 1976; Day and Minster, 1984). This observation led Liu et al. (1976) to use a superposition of several relaxation mechanisms to approximate the nearly constant $Q(w)$. In other

word, the form of stress-strain relationship becomes a convolution equation in case of rock and soil. The solution of such convolutory equation requires very large computational memory and time. Day and Minster (1984) made first attempt to incorporate viscoelastic damping in time-domain FD simulations. Emmerich and Korn (1987) used rheology of generalized Maxwell body (GMB-EK mode) in which n-Maxwell bodies and one Hooke element are connected in parallel. Material dependent anelastic functions were used in the GMB-EK rheological model which poses problem during spatial averaging of material parameters in case of heterogeneous models (Day and Minster, 1984; Emmerich and Korn, 1987). In order to avoid aforesaid problem Kristek and Moczo (2003) derived anelastic function which is independent of material property. Kristek and Moczo (2003) also inferred and recommended the use of harmonic averaging of unrelaxed modulus for an average viscoelastic media.

The prime aim of this paper is the development of an efficient viscoelastic (2,4) staggered-grid finite-difference program based on approximation of velocity-stress viscoelastic SH-wave equations for heterogeneous medium. The validation of implementation of frequency dependent damping in time-domain simulation is done by comparing the numerically computed frequency dependent quality factors and phase velocity with the same computed using GMB-EK rheological model and the Futterman's relations (1962). The spatial spectral damping in homogeneous viscoelastic medium is also computed and compared with the analytical results. The validation of realistic viscoelastic damping in case of heterogeneous medium is also done by comparing the computed soil amplification at fundamental resonance frequency with the analytical one for different soil damping and thickness. The numerical grid-dispersion and stability condition are also analyzed. The computer program is written in FORTRAN with a dynamic memory allocation module so that very large computer memory can be utilized. The module was written in 'i8' environment so that more than 2GB memory can be assigned to a particular array, if required. The VGR-stress imaging technique proposed by Narayan and Kumar (2008) has been used as a free surface boundary condition in order to avoid the thickness discrepancy of first layer by half a vertical grid-size. Furthermore, there is a provision for the use of an improved vacuum formulation proposed by Zeng et al. (2012) as a free surface boundary condition to facilitate the simulation of models containing hill topography. Both the sponge boundary condition of Israeli and Orszag (1981) and absorbing boundary condition of Clayton and Engquist (1977) were implemented on all the three model edges to avoid edge reflections (Kumar and Narayan, 2008).

2. Viscoelastodynamic SH-wave equation

The heterogeneous viscoelastodynamic SH-wave equations based on GMB-EK rheological model using material independent anelastic function (Kristek and Moczo, 2003) are given below,

$$\rho \frac{\partial V}{\partial t} = \frac{\partial \sigma_{xy}}{\partial x} + \frac{\partial \sigma_{zy}}{\partial z} \tag{1}$$

$$\frac{\partial \sigma_{xy}}{\partial t} = \bar{\mu}_u^{xy} \left(\frac{\partial V}{\partial x} \right) - \sum_{l=1}^{m} \bar{Y}_l^{xy} \left(\chi_l^{xy} \right)^{n+\frac{1}{2}}; \qquad l = 1,2,\ldots,m \tag{2}$$

$$\frac{\partial \sigma_{zy}}{\partial t} = \bar{\mu}_u^{zy} \left(\frac{\partial V}{\partial z} \right) - \sum_{l=1}^{m} \bar{Y}_l^{zy} \left(\chi_l^{zy} \right)^{n+\frac{1}{2}}; \qquad l = 1,2,\ldots,m \tag{3}$$

where V is the particle velocity in the y-direction, σ_{xy} and σ_{zy} are the stress components, ρ is the density, χ is the anelastic function and $\bar{\mu}_u$ and $\bar{Y}_l$ are the modified modulus of rigidity and modified anelatic coefficients, respectively. $\frac{\partial}{\partial x}, \frac{\partial}{\partial z} and \frac{\partial}{\partial t}$ are the differential operators. 'm' is the number of relaxation frequency (ω). Superscript 'n' denote the time index. Figure 1 shows the staggering technique, where particle velocity and the density are defined at the nodes and the shear stresses, unrelaxed modulus of rigidity, anelastic coefficients and anelastic functions are defined at the midway between the two adjacent grid points.

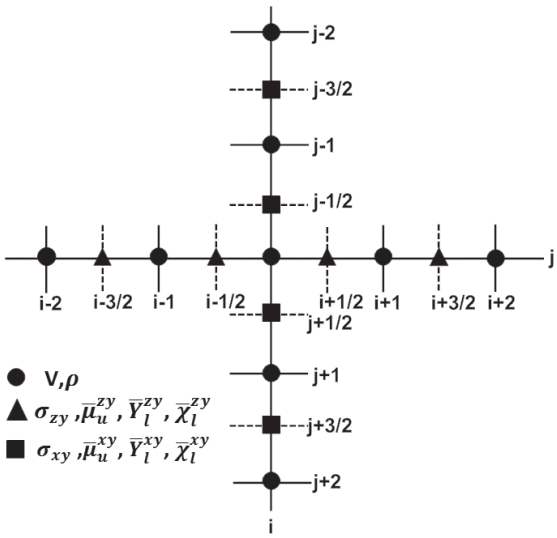

Figure 1. Staggering technique for SH-wave modeling with fourth order spatial accuracy. Particle velocity and density are defined at grid nodes and shear stress components and relaxed modulus of rigidity, anelastic coefficients and anelastic functions are defined at the midway between two adjacent grid points.

There is tremendous increase of required computational memory with the increase of relaxation frequency. Emmerich and Korn (1987) concluded that three relaxation frequencies (m = 3) is sufficient enough based on numerical experiments. Moczo et al. (2004) used four relaxation frequencies (m = 4) in 1D simulation of unbounded homogeneous viscoelstic medium. In the present study, the material independent anelastic functions (χ_l) have been computed at four relaxation frequencies (m = 4) using eqs. (4) and (5).

$$\left(\chi_l^{xy}\right)^{n+\frac{1}{2}} = \frac{2-\Delta t\omega_l}{2+\Delta t\omega_l}\left(\chi_l^{xy}\right)^{n-\frac{1}{2}} + \frac{2\Delta t\omega_l}{2+\Delta t\omega_l}\frac{\partial V}{\partial x} \qquad l=1,2,\ldots,m \tag{4}$$

$$\left(\chi_l^{zy}\right)^{n+\frac{1}{2}} = \frac{2-\Delta t\omega_l}{2+\Delta t\omega_l}\left(\chi_l^{zy}\right)^{n-\frac{1}{2}} + \frac{2\Delta t\omega_l}{2+\Delta t\omega_l}\frac{\partial V}{\partial z} \qquad l=1,2,\ldots,m \tag{5}$$

where Δt is the time step. The modified unrelaxed modulus of rigidity $\overline{\mu}_u^{xy}$ and $\overline{\mu}_u^{zy}$ has been computed using eq. (6).

$$\left.\begin{aligned} \overline{\mu}_u^{xy} &= \mu_u^{xy}\left[1+\sum_{l=1}^{m} G_{1l}Y_l\right] \qquad l=1,2,\ldots,m \\ \overline{\mu}_u^{zy} &= \mu_u^{zy}\left[1+\sum_{l=1}^{m} G_{1l}Y_l\right] \qquad l=1,2,\ldots,m \end{aligned}\right\} \tag{6}$$

Similarly, the modified anelastic coefficients $\overline{Y}_l^{xy}$ and $\overline{Y}_l^{zy}$ can be computed using the following relations

$$\left.\begin{aligned} \overline{Y}_l^{xy} &= 2.G_{2l}\mu_u^{xy}Y_l \qquad l=1,2,\ldots,m \\ \overline{Y}_l^{zy} &= 2.G_{2l}\mu_u^{zy}Y_l \qquad l=1,2,\ldots,m \end{aligned}\right\} \tag{7}$$

where Y_l are anelastic coefficients, μ_u is the unrelaxed modulus and the constants G_{1l} and G_{2l} are given by.

$$G_{1l} = \frac{\Delta t\omega_l}{2-\Delta t\omega_l} \quad \text{and} \quad G_{2l} = \frac{2}{2-\Delta t\omega_l} \qquad l=1,2,\ldots,m \tag{8}$$

The effective values of the unrelaxed modulus of rigidity, μ_u^{xy} and μ_u^{zy} at the midway between the two adjacent grid points, are obtained using harmonic mean of μ_u at the node points in order to incorporate the material discontinuity (Moczo et al., 2002).

$$\left(\mu_{\mathrm{u}}^{\mathrm{xy}}\right)_{\mathrm{i}+\frac{1}{2},\mathrm{j}} = \left[\frac{1}{2}\left(\frac{1}{\left(\mu_{\mathrm{u}}\right)_{\mathrm{i,j}}} + \frac{1}{\left(\mu_{\mathrm{u}}\right)_{\mathrm{i+1,j}}}\right)\right]^{-1} \text{ and } \left(\mu_{\mathrm{u}}^{\mathrm{zy}}\right)_{\mathrm{i,j}+\frac{1}{2}} = \left[\frac{1}{2}\left(\frac{1}{\left(\mu_{\mathrm{u}}\right)_{\mathrm{i,j}}} + \frac{1}{\left(\mu_{\mathrm{u}}\right)_{\mathrm{i,j+1}}}\right)\right]^{-1} \quad (9)$$

Further, the unrelaxed modulus has been obtained using phase velocity of S-wave (V_{S,ω_r}) at reference frequency (ω_r) and eqs. (10) and (11) (Moczo et al., 1997).

$$\mu_u = \rho V_{S,w_r}^2 \frac{R+\vartheta_1}{2R^2} \qquad \text{where} \quad R = \sqrt{\vartheta_1^2 + \vartheta_2^2} \quad (10)$$

$$\vartheta_1 = 1 - \sum_{l=1}^{m}\left[Y_l \frac{1}{1+\left(\frac{\omega_r}{\omega_l}\right)^2}\right] \quad \vartheta_2 = \sum_{l=1}^{m}\left[Y_l \frac{\frac{\omega_r}{\omega_l}}{1+\left(\frac{\omega_r}{\omega_l}\right)^2}\right] \quad l = 1,2,\ldots,m \quad (11)$$

Anelastic coefficients Y_l, $l = 1,2,\ldots,m$ have been computed using following equation with the help of Futterman's equation (Futterman, 1962) and least square technique.

$$Q^{-1}(\omega_k) = \sum_{l=1}^{m} \frac{\omega_l\omega_k + Q^{-1}(\omega_k)\omega_l^2}{\omega_l^2 + \omega_k^2} Y_l \quad l = 1,2,\ldots,m \quad k = 1,2,\ldots,2m-1 \quad (12)$$

The logarithmically distributed considered values of relaxation frequencies ω_1, ω_2, ω_3 and ω_4 are 0.3141, 3.141, 31.41 and 314.1, respectively. The $Q(\omega_k)$ values obtained using the Q at reference frequency and Futterman's equation has been used for optimization. The ω_k values are also logarithmically distributed. ω_k is defined at ω_l as well as at the mid of two consecutive ω_l values. Further, $\omega_{k=1}$ was equal to $\omega_{l=1}$ and $\omega_{k=2m-1}$ was equal to $\omega_{l=m}$.

3. Finite-difference approximation

In equations (1)–(3), the time derivative was replaced by second order accurate central difference FD operator and space derivatives were replaced by a fourth order staggered grid FD operator (Levander, 1988; Graves, 1996; Moczo et al., 2000; Narayan and Kumar, 2008).

$$V_{i,j}^{n+\frac{1}{2}} = V_{i,j}^{n-\frac{1}{2}} + \frac{2\Delta t}{\rho_{i,j}\left(\Delta \mathrm{X}_{\mathrm{i-1,j}} + \Delta \mathrm{X}_{\mathrm{i,j}}\right)}\left[a\left\{\left(\sigma_{xy}\right)_{i+\frac{1}{2},j}^{n} - \left(\sigma_{xy}\right)_{i-\frac{1}{2},j}^{n}\right\} + b\left\{\left(\sigma_{xy}\right)_{i+\frac{3}{2},j}^{n} - \left(\sigma_{xy}\right)_{i-\frac{3}{2},j}^{n}\right\}\right] +$$

$$\frac{2\Delta t}{\rho_{i,j}(\Delta \mathrm{Z}_{\mathrm{i,j-1}} + \Delta \mathrm{Z}_{\mathrm{i,j}})}\left[a\left\{\left(\sigma_{zy}\right)_{i,j+\frac{1}{2}}^{n} - \left(\sigma_{zy}\right)_{i,j-\frac{1}{2}}^{n}\right\} + b\left\{\left(\sigma_{zy}\right)_{i,j+\frac{3}{2}}^{n} - \left(\sigma_{zy}\right)_{i,j-\frac{3}{2}}^{n}\right\}\right] \quad (13)$$

$$\left(\sigma_{xy}\right)_{i+\frac{1}{2},j}^{n+1}=\left(\sigma_{xy}\right)_{i,j+\frac{1}{2}}^{n}+\frac{\Delta t}{\Delta \mathrm{X}_{\mathrm{i,j}}}\left(\bar{\mu}_{u}^{xy}\right)_{i+\frac{1}{2},j}\left[a\left\{V_{i+1,j}^{n+\frac{1}{2}}-V_{i,j}^{n+\frac{1}{2}}\right\}+b\left\{V_{i+2,j}^{n+\frac{1}{2}}-V_{i-1,j}^{n+\frac{1}{2}}\right\}\right]-$$

$$\Delta t\left[\left(\bar{Y}_{1}^{xy}\right)_{i+\frac{1}{2},j}\left(\chi_{1}^{xy}\right)_{i+\frac{1}{2},j}^{n+\frac{1}{2}}+\left(\bar{Y}_{2}^{xy}\right)_{i+\frac{1}{2},j}\left(\chi_{2}^{xy}\right)_{i+\frac{1}{2},j}^{n+\frac{1}{2}}+\left(\bar{Y}_{3}^{xy}\right)_{i+\frac{1}{2},j}\left(\chi_{3}^{xy}\right)_{i+\frac{1}{2},j}^{n+\frac{1}{2}}+\left(\bar{Y}_{4}^{xy}\right)_{i+\frac{1}{2},j}\left(\chi_{4}^{xy}\right)_{i+\frac{1}{2},j}^{n+\frac{1}{2}}\right] \quad (14)$$

$$\left(\sigma_{zy}\right)_{i,j+\frac{1}{2}}^{n+1}=\left(\sigma_{zy}\right)_{i,j+\frac{1}{2}}^{n}+\frac{\Delta t}{\Delta \mathrm{Z}_{\mathrm{i,j}}}\left(\bar{\mu}_{u}^{zy}\right)_{i,j+\frac{1}{2}}\left[a\left\{V_{i,j+1}^{n+\frac{1}{2}}-V_{i,j}^{n+\frac{1}{2}}\right\}+b\left\{V_{i,j+2}^{n+\frac{1}{2}}-V_{i,j-1}^{n+\frac{1}{2}}\right\}\right]-$$

$$\Delta t\left[\left(\bar{Y}_{1}^{zy}\right)_{i,j+\frac{1}{2}}\left(\chi_{1}^{zy}\right)_{i,j+\frac{1}{2}}^{n+\frac{1}{2}}+\left(\bar{Y}_{2}^{zy}\right)_{i,j+\frac{1}{2}}\left(\chi_{2}^{zy}\right)_{i,j+\frac{1}{2}}^{n+\frac{1}{2}}+\left(\bar{Y}_{3}^{zy}\right)_{i,j+\frac{1}{2}}\left(\chi_{3}^{zy}\right)_{i,j+\frac{1}{2}}^{n+\frac{1}{2}}+\left(\bar{Y}_{4}^{zy}\right)_{i,j+\frac{1}{2}}\left(\chi_{4}^{zy}\right)_{i,j+\frac{1}{2}}^{n+\frac{1}{2}}\right] \quad (15)$$

The value of constants '*a*' and '*b*' are 9/8 and –1/24, respectively. The superscript '*n*' refers to the time index and the subscript '*i*' and '*j*' refers to the spatial indices in the *x* and *z* direction, respectively. $\Delta X_{i,j}$ and $\Delta Z_{i,j}$ are the grid size at grid position '*i*, *j*' in *x*- and *z*-direction, respectively.

FD Approximation of anelastic functions χ_l^{xy} and χ_l^{zy} is given by

$$\left.\begin{aligned}
\left(\chi_{1}^{xy}\right)_{i+\frac{1}{2},j}^{n+\frac{1}{2}}&=F_{11}\left(\chi_{1}^{xy}\right)_{i+\frac{1}{2},j}^{n-\frac{1}{2}}+\frac{0.5F_{21}}{\Delta x_{i,j}}\left[a\left\{V_{i+1,j}^{n+\frac{1}{2}}-V_{i,j}^{n+\frac{1}{2}}\right\}+b\left\{V_{i+2,j}^{n+\frac{1}{2}}-V_{i-1,j}^{n+\frac{1}{2}}\right\}\right]\\
\left(\chi_{2}^{xy}\right)_{i+\frac{1}{2},j}^{n+\frac{1}{2}}&=F_{12}\left(\chi_{1}^{xy}\right)_{i+\frac{1}{2},j}^{n-\frac{1}{2}}+\frac{0.5F_{22}}{\Delta x_{i,j}}\left[a\left\{V_{i+1,j}^{n+\frac{1}{2}}-V_{i,j}^{n+\frac{1}{2}}\right\}+b\left\{V_{i+2,j}^{n+\frac{1}{2}}-V_{i-1,j}^{n+\frac{1}{2}}\right\}\right]\\
\left(\chi_{3}^{xy}\right)_{i+\frac{1}{2},j}^{n+\frac{1}{2}}&=F_{13}\left(\chi_{1}^{xy}\right)_{i+\frac{1}{2},j}^{n-\frac{1}{2}}+\frac{0.5F_{23}}{\Delta x_{i,j}}\left[a\left\{V_{i+1,j}^{n+\frac{1}{2}}-V_{i,j}^{n+\frac{1}{2}}\right\}+b\left\{V_{i+2,j}^{n+\frac{1}{2}}-V_{i-1,j}^{n+\frac{1}{2}}\right\}\right]\\
\left(\chi_{4}^{xy}\right)_{i+\frac{1}{2},j}^{n+\frac{1}{2}}&=F_{14}\left(\chi_{4}^{xy}\right)_{i+\frac{1}{2},j}^{n-\frac{1}{2}}+\frac{0.5F_{24}}{\Delta x_{i,j}}\left[a\left\{V_{i+1,j}^{n+\frac{1}{2}}-V_{i,j}^{n+\frac{1}{2}}\right\}+b\left\{V_{i+2,j}^{n+\frac{1}{2}}-V_{i-1,j}^{n+\frac{1}{2}}\right\}\right]
\end{aligned}\right\} \quad (16)$$

$$\left.\begin{aligned}
\left(\chi_{1}^{zy}\right)_{i,j+\frac{1}{2}}^{n+\frac{1}{2}}&=F_{11}\left(\chi_{1}^{zy}\right)_{i,j+\frac{1}{2}}^{n-\frac{1}{2}}+\frac{0.5F_{21}}{\Delta z_{i,j}}\left[a\left\{V_{i,j+1}^{n+\frac{1}{2}}-V_{i,j}^{n+\frac{1}{2}}\right\}+b\left\{V_{i,j+2}^{n+\frac{1}{2}}-V_{i,j-1}^{n+\frac{1}{2}}\right\}\right]\\
\left(\chi_{2}^{zy}\right)_{i,j+\frac{1}{2}}^{n+\frac{1}{2}}&=F_{12}\left(\chi_{1}^{zy}\right)_{i,j+\frac{1}{2}}^{n-\frac{1}{2}}+\frac{0.5F_{22}}{\Delta z_{i,j}}\left[a\left\{V_{i,j+1}^{n+\frac{1}{2}}-V_{i,j}^{n+\frac{1}{2}}\right\}+b\left\{V_{i,j+2}^{n+\frac{1}{2}}-V_{i,j-1}^{n+\frac{1}{2}}\right\}\right]
\end{aligned}\right\}$$

$$\left.\begin{aligned}
\left(\chi_3^{zy}\right)_{i,j+\frac{1}{2}}^{n+\frac{1}{2}} &= F_{13}\left(\chi_1^{zy}\right)_{i,j+\frac{1}{2}}^{n-\frac{1}{2}} + \frac{0.5F_{23}}{\Delta z_{i,j}}\left[a\left\{V_{i,j+1}^{n+\frac{1}{2}} - V_{i,j}^{n+\frac{1}{2}}\right\} + b\left\{V_{i,j+2}^{n+\frac{1}{2}} - V_{i,j-1}^{n+\frac{1}{2}}\right\}\right] \\
\left(\chi_4^{zy}\right)_{i,j+\frac{1}{2}}^{n+\frac{1}{2}} &= F_{14}\left(\chi_4^{zy}\right)_{i,j+\frac{1}{2}}^{n-\frac{1}{2}} + \frac{0.5F_{24}}{\Delta z_{i,j}}\left[a\left\{V_{i,j+1}^{n+\frac{1}{2}} - V_{i,j}^{n+\frac{1}{2}}\right\} + b\left\{V_{i,j+2}^{n+\frac{1}{2}} - V_{i,j-1}^{n+\frac{1}{2}}\right\}\right]
\end{aligned}\right\} \quad (17)$$

The functions $F_{11}-F_{14}$ and $F_{21}-F_{24}$ can be obtained using following relations

$$\left.\begin{aligned}
F_{11} &= \frac{2-\omega_1\Delta t}{2+\omega_1\Delta t} & F_{21} &= \frac{\omega_1\Delta t}{2+\omega_1\Delta t} \\
F_{12} &= \frac{2-\omega_2\Delta t}{2+\omega_2\Delta t} & F_{22} &= \frac{\omega_2\Delta t}{2+\omega_2\Delta t} \\
F_{13} &= \frac{2-\omega_3\Delta t}{2+\omega_3\Delta t} & F_{23} &= \frac{\omega_3\Delta t}{2+\omega_3\Delta t} \\
F_{14} &= \frac{2-\omega_4\Delta t}{2+\omega_4\Delta t} & F_{24} &= \frac{\omega_4\Delta t}{2+\omega_4\Delta t}
\end{aligned}\right\} \quad (18)$$

4. Validation of FD program

In order to validate the accuracy of FD program and the implementation of viscoelastic damping in time-domain simulation, seismic responses of an unbounded homogeneous viscoelastic model and a bounded heterogeneous viscoelastic model were simulated and analysed. The stability and grid-dispersion are also studied.

4.1. Numerical grid-dispersion and stability

To study the numerical grid-dispersion, responses of an unbounded homogeneous elastic half-space model with V_S = 3200 m/s and density ρ = 2.8 g/cm^3 were computed. A Ricker wavelet with 4.0 Hz dominant frequency with considerable spectral amplitude in a frequency range of 0.25 Hz to 10.0 Hz was used as an excitation function for generating a horizontal linear source. A linear source was inserted into the numerical grid using various point sources at a particular horizon keeping five point sources per- dominant wavelength. Model was discretised using square grids of size 60 m. Seismic response at two location on a vertical array was computed using time step Δt = 0.012 sec. The numerical dispersion curve was developed by plotting a graph between the normalized phase-

velocity (V^{grid}/V) and the number of grid point per wavelength ($\lambda/\Delta z$). V^{grid} is the phase-velocity computed numerically using the Fourier transform of seismic responses at two locations 60 m apart, recorded in the direction of source. The phase-velocity was computed using phase-difference $\Delta\varphi(\omega)$ and the following equation

$$V^{grid}(\omega) = \frac{\omega \Delta x}{\Delta\varphi(\omega)}. \tag{19}$$

Figure 2 shows the comparison of numerical dispersion curve with analytical dispersion curve obtained using the relationship given by Moczo et al. (2000). A good agreement between the two curves reveals that the error in the numerically computed dispersion curve is within the permissible limit when the number of grids per shortest wavelength is more than 6.

The stability condition for the (2, 4) SH-wave FD algorithm was obtained based on various iterative simulations for a viscoelastic model. The S-wave velocity computed using unrelaxed moduli gives the largest velocity for the considered model parameters and frequency bandwidth. This largest S-wave velocity can be conservatively used for computing the stability condition. It was finally con-

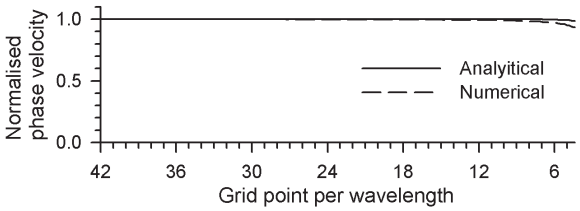

Figure 2. A comparison of numerical and analytical grid dispersion curves for the SH-wave.

cluded that the scheme is stable if the following stability condition is locally satisfied.

$$\frac{V_{Smax}\Delta t}{min(\Delta x,\ \Delta z)} \leq 0{,}7 \tag{20}$$

where V_{Smax} is the maximum S-wave velocity, Δx and Δz are the grid size in x- and z-directions at a particular node.

4.2. Computation of phase velocity and quality factor

The accuracy of implementation of frequency-dependent damping in time-domain is validated based on a comparison of numerically computed phase velocity $V_S(\omega)$ and quality factor $Q(\omega)$ with the same computed using Futterman's

Table 1. Quality factors (Q) and unrelaxed rigidity (μ) for various unbounded homogeneous viscoelastic models (HVM1-HVM3) with a common velocity at reference frequency as 3200 m/s and density 2800 kg/m^3.

S.N.	Model parameters	HVM1	HVM2	HVM3
1	Quality factor at F_R	320	160	80
2	Unrelaxed rigidity (GPa)	28.935	29.201	29.744

relations and the GMB-EK model for an unbounded homogeneous viscoelastic medium. In order to fulfil this aim, the responses of an unbounded model were computed at two offsets on a vertical array for different rheology of the medium. The S-wave velocity and quality factor at reference frequency (F_r = 1 Hz), density and unrelaxed modulus of rigidity for different homogeneous viscoelastic models (HVM1-HVM3) are given in Tab. 1. The rheology of medium is varied by changing the quality factor at reference frequency and at the same time keeping other parameters constant. The four relaxation frequencies used in the computations were taken as 0.02 Hz, 0.2 Hz, 2.0 Hz and 20 Hz.

The Fourier transform of seismic responses at two locations 10 m apart were used for the computation of phase velocity numerically. The phase velocity was also computed analytically using GMB-EK model. In case of GMB-EK model, the relaxed modulus of rigidity at different frequency was computed using following equation (Moczo et al., 1997).

$$\mu(\omega) = \mu_{\mathrm{u}}\left[1 - \sum_{l=1}^{m} Y_l \frac{{\omega_l}^2}{{\omega_l}^2 + \omega^2}\right] \tag{22}$$

Figure 3 shows a comparison of phase-velocity computed numerically for different models and analytically using GMB-EK model and the Futterman's relationship. Analysis of Fig. 3 reveals an excellent agreement between the numerically computed phase-velocity and the phase velocity computed using Futterman's relation and GMB-EK model.

The frequency dependent quality factors were numerically computed using phase velocity $V_S(\omega)$ and the amplitude spectra of particle velocity $V(x,\omega)$ time history at two locations and the following relationship.

$$\frac{1}{Q(\omega)} = -\frac{2V_S(\omega)}{\omega \Delta \mathrm{z}}\left[ln\left|V(z+\Delta z,\omega)\right| - ln\left|V(z,\omega)\right|\right] \tag{23}$$

$\left|V(z,\omega)\right|$ is the mod of Fourier amplitude spectra of particle velocity at a distance of z and $z + \Delta z$ from the line source.

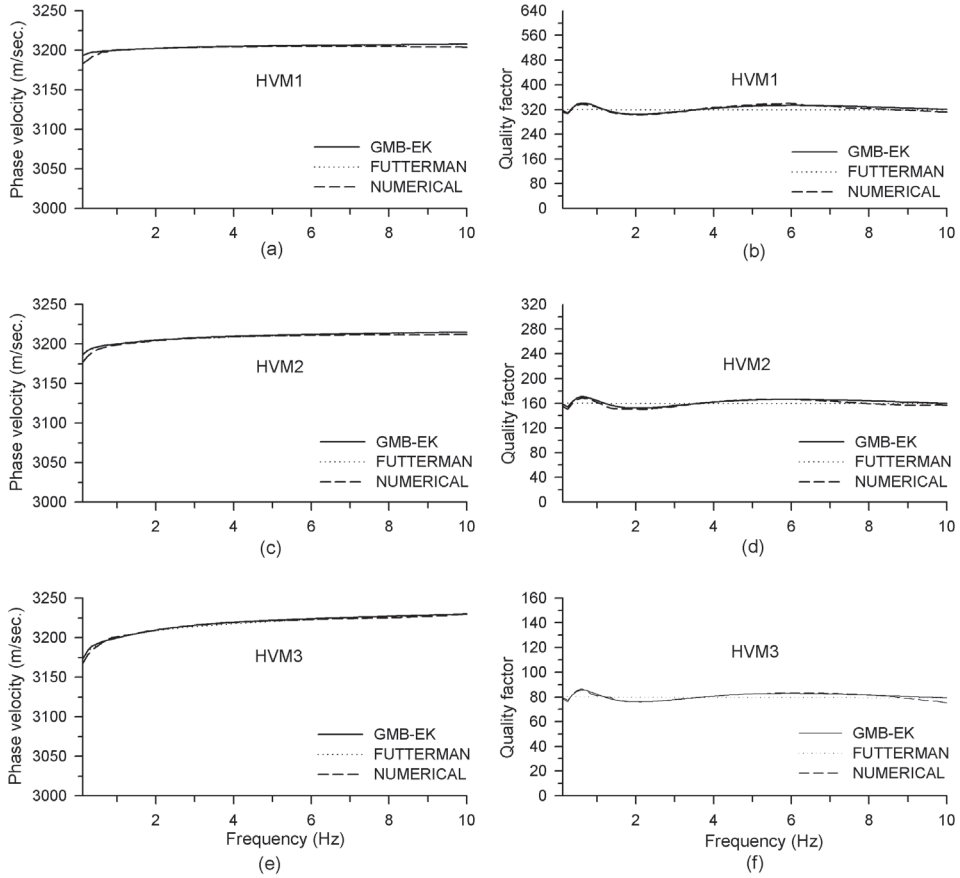

Figure 3. Comparison of numerically computed phase velocity (*a*, *c* and *e*) and quality factor (*b*, *d* and *f*) in an unbounded homogeneous viscoelastic medium with the same computed analytically using Futterman's relations and the GMB-EK rheological model.

The frequency dependent quality factors were also computed analytically using GMB-EK model with the help of following equation.

$$\frac{1}{Q(\omega)} = \sum_{l=1}^{m} Y_l \frac{\omega\,\omega_l}{\omega_l^{\,2} + \omega^2} \Big/ \left[1 - \sum_{l=1}^{m} Y_l \frac{\omega_l^{\,2}}{\omega_l^{\,2} + \omega^2} \right] \tag{24}$$

A comparison of quality factor computed numerically and analytically using GMB-EK model and the Futterman's relationship is also shown in Fig. 3b. An excellent agreement between the numerically computed quality factor and phase-

velocity and the same computed using Futterman's relation and GMB-EK model validates the accuracy of implementation of realistic damping in the developed FD algorithm for time domain simulations.

The accuracy of implementation of viscoelastic damping was also verified based on comparison of spatial frequency dependent damping results with the same computed analytically using phase-velocity and quality factors obtained from Futterman's relationship and GMB-EK model. The seismic responses of e same model parameters were computed at different offsets from the linear horizontal source. The spectral amplitude ratios A_z / A_0 were computed for different distance travelled (z). The trace recorded nearest to the linear source was used as a reference distance ($z = 0$). The spectral amplitude ratios for the same distance travelled were also computed using the phase-velocity and quality factors obtained using Futterman's relation and GMB-EK model and the following relation.

$$\frac{A_z}{A_0} = e^{-\frac{\omega z}{2Q(\omega)V_S(\omega)}} \tag{25}$$

Figure 4 shows a comparison of numerically computed spectral amplitude ratio A_z / A_0 for distance travelled as 1500 m, 3000 m, 4500 m and 6000 m and the same computed using phase-velocity and quality factors obtained using Futterman's relationship and GMB-EK model. The spectral amplitude ratio A_z / A_0 in case of FD method was obtained just by taking the ratio of spectra of seismic responses at two offsets since there is no divergence effect. The excellent matching of analytically and numerically computed spectral amplitude ratios also validates the accuracy of procedure of implementation of realistic damping in the developed time domain SH-wave finite-difference algorithm.

4.3. Response of bounded heterogeneous viscoelastic model

In order to further validate the accuracy of implementation of realistic damping in heterogeneous medium, seismic response of a bounded model containing a horizontal soil layer over the half-space was simulated. VGR-stress imaging technique was used as a free surface boundary condition (Narayan and Kumar, 2008; 2010). Rheology of soil was changed just by only taking the different value of quality factor at reference frequency. The parameters like velocity and quality factors at reference frequency (F_r), soil thickness, density and unrelaxed modulus of rigidity for soil layer for different considered models (SRM1-SRM3) are given in Tab. 2. The respective parameters for the basement were the same as that of HVM1 model of the previous case (Tab. 1). Figure 5a depicts the simulated seismic responses of half-space (without soil layer) and various heterogeneous viscoelastic models (SRM1-SRM3).

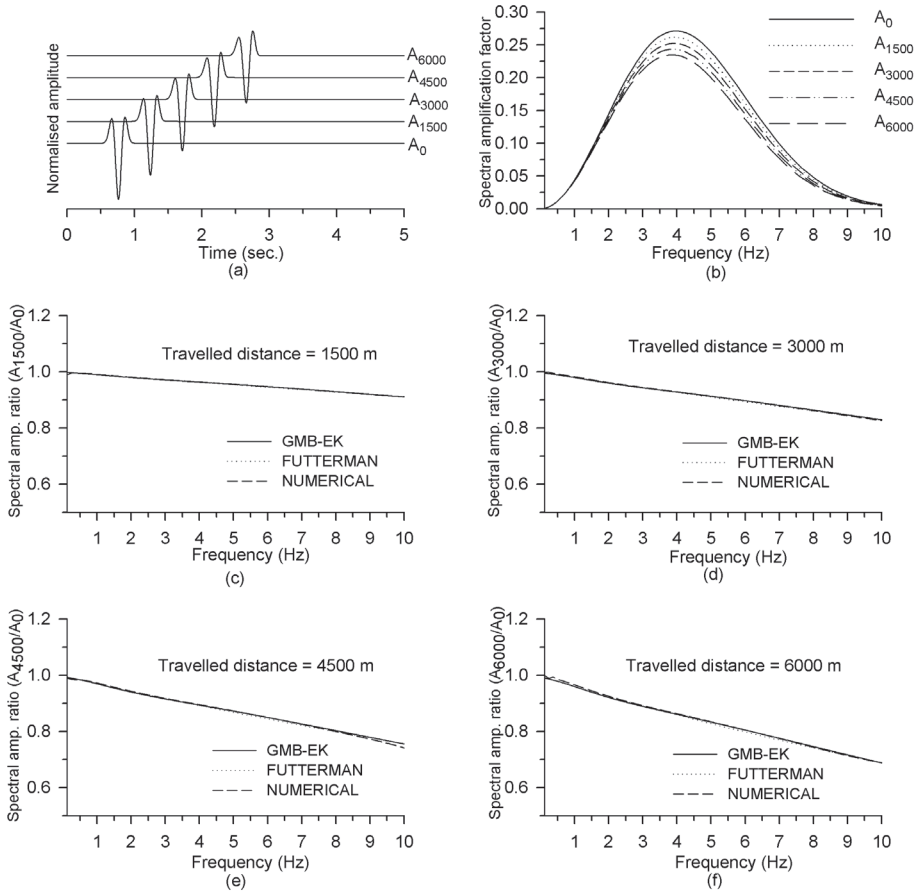

Figure 4. A comparison of numerically computed spectral amplitude ratio for different distance travelled by SH-wave in an unbounded homogeneous viscoelastic medium with the same computed analytically using Futterman's relations and the GMB-EK rheological model.

Table 2. Quality factors (Q) and unrelaxed rigidity (μ) for soil considered in various inhomogeneous viscoelastic models (SRM1-SRM3) with a common velocity at reference frequency as 525 m/s, density 2000 kg/m^3 and soil thickness 40 m. This table also shows a comparison of obtained fundamental frequency (F_0) and spectral amplification at F_0 (SAF) with the analytical one.

Model	Q at F_R	μ (GPa)	F_0 (Hz)		*SAF*	
			Numerical	Analytical	Numerical	Analytical
SRM1	10	7.476	3.40	3.40	4.90	4.92
SRM2	20	6.401	3.33	3.34	6.14	6.28
SRM3	50	5.847	3.29	3.30	7.35	7.48

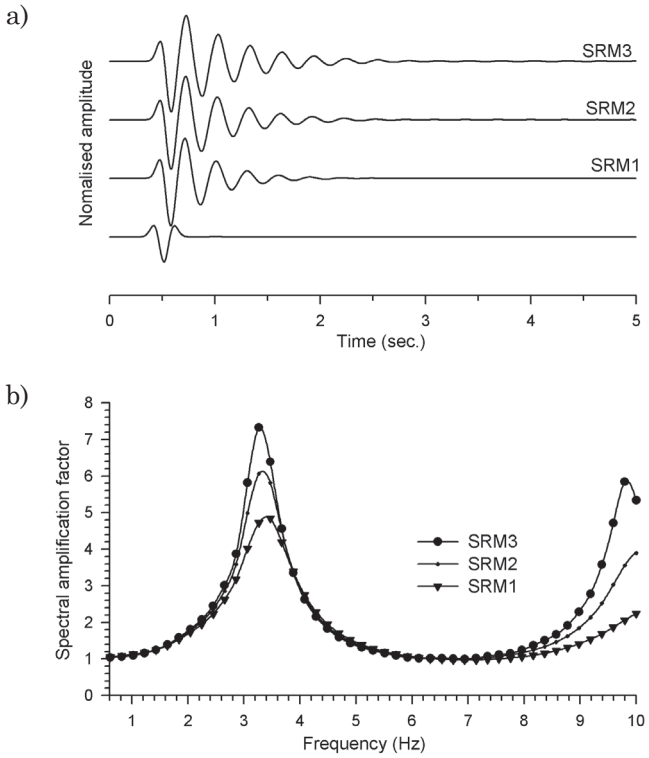

Figure 5. (*a*) 1D seismic responses of models with a different soil damping and half-space and (*b*) spectral amplification factors, respectively.

The spectral soil amplification was computed just by taking the ratio of spectra of response of model containing soil layer with the response corresponding to homogeneous half-space. Figure 5b depicts that the spectral amplification factors are very much dependent on the damping in soil layer. The analysis of this figure reveals a decrease of spectral amplification with the increase of damping in the soil layer. This figure also depicts the increase of fundamental and higher mode frequencies with the increase of damping in the soil. This finding corroborates with the GMB-EK rheology and Futterman's relationship where there is increase of phase velocity with the increase of damping. The spectral amplifications at fundamental resonance frequency (*SAF*) were computed analytically using the phase velocity $V_S(\omega)$ and quality factor $Q(\omega)$ corresponding to GBM-EK model and the following relationship (Bard and Riepl-Thomas, 2000)

$$SAF = \frac{IC}{1 + \frac{\pi}{4}\frac{IC}{Q(\omega)}} \tag{26}$$

where *IC* is impedance contrast between soil layer and the half-space. A comparison of numerically obtained fundamental frequency (F_0) and spectral amplification at this frequency (*SAF*) with analytical solutions reveals an excellent matching (Tab. 2).

Seismic responses of the SRM2 model (Tab. 2) were also computed for different thickness of soil layer. Figure 6a shows the seismic responses for soil

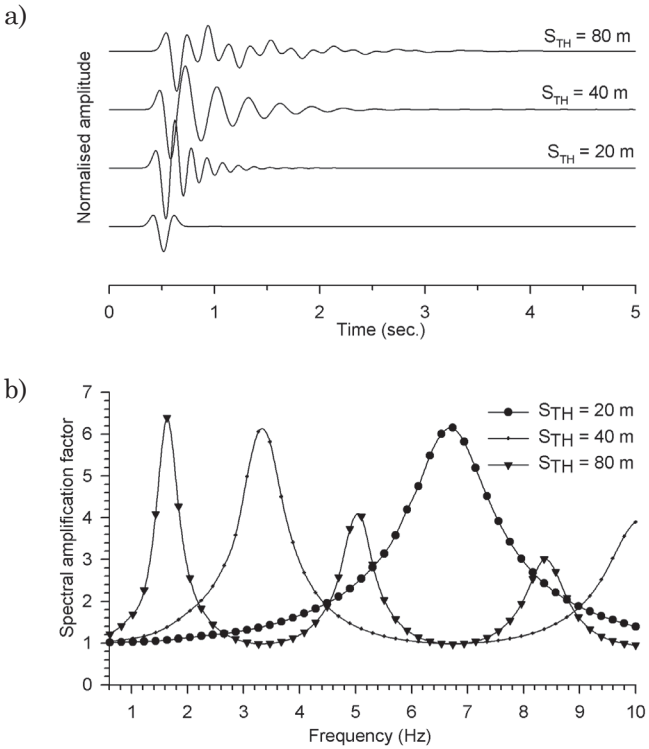

Figure 6. (*a*) Seismic responses of SRM2 model (Tab. 2) with different soil thickness as well as half-space and (*b*) spectral amplification factors, respectively.

Table 3. Different soil thickness (S_{TH}) used in SRM2 model (Tab. 2) and a comparison of obtained fundamental frequency (F_0) and spectral amplification at F_0 (SAF) with the analytical one.

S.N.	Soil thickness (S_{TH}) (m)	F_0 (Hz)		SAF	
		Numerical	Analytical	Numerical	Analytical
1.	20	6.71	6.76	6.16	6.22
2.	40	3.33	3.34	6.14	6.28
3.	80	1.63	1.65	6.40	6.34

thickness as 20 m, 40 m and 80 m. The spectral amplification factors for different thickness of soil layer are shown in Fig. 6b. A comparison of numerically obtained F_0 and *SAF* with the analytical one is given in Tab. 3. An excellent matching of numerically computed F_0 and *SAF* with the analytical one for different soil damping and soil thickness further validates the accuracy of procedure of implementation of realistic viscoelastic damping in the time domain finite-difference simulations.

5. Discussion and conclusions

A forth-order spatial accurate viscoelastic SH-wave staggered grid FD computer program is developed based on the GMB-EK rheological model using material independent anelastic function (Emmerich and Korn, 1987; Kristek and Moczo, 2003). Grid-dispersion and stability analysis reveals that the requirement of number of grids per-wavelength and stability condition are the same as reported by others (Moczo et. al., 2000). The excellent matching of numerically computed phase-velocity and quality factor for an unbounded viscoelastic homogeneous medium with the same computed analytically using GMB-EK rheological model and Futterman's relation (1962) validates the accuracy of implementation of realistic viscoelastic damping in the time-domain FD algorithm. Further, an excellent matching of obtained fundamental frequency of soil layer and the spectral amplification at the same frequency for different values of soil damping and thickness with the analytical results (Bard and Riepl-Thomas, 2000) also reflects the efficiency and accuracy of developed program for simulating the response of heterogeneous viscoelastic medium.

The inquiries about the program availability, hardware and software requirements, as well as compilation or usage details may be requested from the first author.

Acknowledgement – The first author is grateful to the Council of Scientific and Industrial Research, New Delhi for financial assistance through Grant Number CSR-569-EQD.

References

Bard, P. Y. and Riepl-Thomas, J. (2000): Wave propagation in complex geological structures and their effects on strong ground motion, in: *Advances in earthquake engineering-wave motion in earthquake engineering*, edited by Kausel, E. and Manolis, G. D., 37–95, ISBN: 978-1-85312-744-1.

Clayton, R. W. and Engquist, B. (1977): Absorbing boundary conditions for acoustic and elastic wave equations, Bull. Seism. Soc. Am., **67**, 1529–1540.

Day, S. M. and Minster, J. B. (1984): Numerical simulation of wavefields using a Padé approximant method, *Geophys. J. Roy. Astr. S.*, **78**, 105–118.

Emmerich, H. and Korn, M. (1987): Incorporation of attenuation into time-domain computations of seismic wave fields, *Geophysics*, **52**, 1252–1264, DOI: 10.1190/1.1442386.

Futterman, W. I. (1962): Dispersive body waves, *J. Geophys. Res.*, **67**, 5279–5291, DOI: 10.1029/JZ067i013p05279.

Graves, R. W. (1996): Simulating seismic wave propagation in 3D elastic media using staggered-grid finite differences, *Bull. Seism. Soc. Am.*, **86**, 1091–1106.

Israeli, M. and Orszag, S. A. (1981): Approximation of radiation boundary conditions, J. Comput. Phys., **41**, 115–135, DOI: 10.1016/0021-9991(81)90082-6.

Kristeck, J. and Moczo, P. (2003): Seismic wave propagation in viscoelastic media with material disconuties – a 3D 4th order staggered grid finite difference modeling, *Bull. Seism. Soc. Am.*, **93**, 2273–2280.

Kumar, S. and Narayan, J. P. (2008): Implementation of absorbing boundary conditions in a 4th order accurate SH-wave staggered grid finite difference program with variable grid size, *Acta Geophys.*, **56**, 1090–1108, DOI: 10.2478/s11600-008-0043-9.

Levander, A. R. (1988): Fourth-order finite-difference P-SV seismograms, *Geophysics*, **53**, 1425–1436, DOI: 10.1190/1.1442422.

Liu, H. P., Anderson, D. L. and Kanamori, H. (1976): Velocity dispersion due to anelasticity; implications for seismology and mantle composition, *Geophys. J. Roy. Astr. S.*, **47**, 41–58.

Madariaga, R. (1976): Dynamic of an expanding circular fault, *Bull. Seism. Soc. Am.*, **65**, 163–182.

McDonal, F. J., Angona, F. A., Mills, L. R., Sengbush, R. L., Van Nostrand, R. G. and White, J. E. (1958): Attenuation of shear and compressional waves in Pierre shale, *Geophys.*, **23**, 421–439, DOI: 10.1190/1.1438489.

Moczo, P., Bystrický, E., Kristek, J., Carcione, J. M. and Bouchon, M. (1997): Hybrid modelling of P-SV seismic motion at inhomogeneous viscoelastic topographic structures, Bull. Seism. Soc. Am., **87**, 1305–1323.

Moczo, P., Kristek, J., Vavryčuk, V., Archuleta, R. J. and Halada, L. (2002): 3D heterogeneous staggered-grid finite-difference modelling of seismic motion with volume harmonic and arithmetic averaging of elastic moduli and densities, *Bull. Seism. Soc. Am.*, **92**, 3042–3066.

Moczo, P., Kristek, J. and Halada, L. (2004): *The finite-difference method for seismologists. An introduction*. Comenius University, Bratislava, ISSN: 80-223-2000-5, 155 pp.

Moczo, P., Kristek, J. and Bystricky, E. (2000): Stability and grid dispersion of the P-SV 4th order staggered grid finite difference scheme, Stud. Geophys. Geod., **44**, 381–402.

Narayan, J. P. (2003): 2.5D simulation of ridge-weathering effects on the ground motion characteristics*, J. of Earthquake Eng.*, **7**, 447–461.

Narayan, J. P. and Rao P. V. Prasad (2003): Two and half dimensional simulation of ridge effects on the ground motion characteristics, *Pure App. Geophys.*, **160**, 1557–1571, DOI: 10.1007/s00024-003-2360-x.

Narayan, J. P. (2005): Study of basin-edge effects on the ground motion characteristics using 2.5-D modeling, Pure App. Geophys., **162**, 273–289, DOI: 10.1007/s00024-004-2600-8.

Narayan, J. P. and Kumar, S. (2008): A fourth order accurate SH-wave staggered grid finite-difference program with variable grid size and VGR-stress imaging technique, Pure App. Geophys., **165**, 271–294, DOI: 10.1007/s00024-008-0298-8.

Narayan, J. P., and Kumar, S. (2010): A 4th order accurate P-SV wave staggered grid finite difference algorithm with variable grid size and VGR-stress imaging technique *Geofizika*, **27**, 45–68.

Narayan, J. P. (2010): Effects of impedance contrast and soil thickness on the basin transduced Rayleigh waves and associated differential ground motion, *Pure Appl. Geophys.*, **167**, 1485–1510, DOI: 10.1007/s00024-010-0131-z.

Narayan, J. P. (2012): Effects of P-wave and S-wave impedance contrast on the characteristics of basin transduced Rayleigh waves, Pure App. Geophys., **169**, 693–709, DOI: 10.1007/s00024-011-0338-7.

Zeng, C., J. Xia, R. Miller and G. Tsoflias (2012): An improved vacuum formulation for 2D finite-difference modeling of Rayleigh waves including surface topography and internal discontinuities, *Geophys.*, **77**(1), T1–T9, DOI: 10.2113/JEEG17.3.129.

SAŽETAK

Program konačnih razlika četvrtog reda točnosti za simulaciju rasprostiranja SH-vala u heterogenom viskoelastičnom sredstvu

J. P. Narayan i Vinay Kumar

Prikazan je program konačnih razlika (FD) na razmaknutoj mreži u vremenskoj domeni za simulaciju rasprostiranja SH-vala u viskoelastičnom heterogenom sredstvu. Uključivanje realističnog prigušenja u program temelji se na reološkom modelu poznatom kao generalizirano Maxwellovo tijelo (GMB-EK). Valjanost implementiranog prigušenja je potvrđena usporedbom numerički dobivenih frekventno ovisnih kvalitativnih faktora i fazne brzine s onima izračunatim GMB-EK reološkim modelom i korištenjem Futtermanove relacije. Točnost je potvrđena i usporedbom numerički izračunate amplifikacije tla pri rezonantnoj frekvenciji za različito prigušenje s analitičkim rješenjima. Stabilnost i disperzija mreže su također detaljno istraženi.

Corresponding author's address: J. P. Narayan, Department of Earthquake Engineering, Indian Institute of Technology Roorkee, Roorkee-247667, India, email: jaypnfeq@iitr.ernet.in